X-734-67-368

NASA TM X-55869

OPTIMAL CONTROL APPLICATIONS FOR ELECTROTHERMAL MULTIJET SYSTEMS ON SYNCHRONOUS EARTH SPACECRAFT

WILLIAM C. ISLEY

AUGUST 1967

GODDARD SPACE FLIGHT CENTER

GREENBELT, MARYLAND

Submitted to AIAA Electric Propulsion and Plasmadynamics Conference September 11-13 Colorado Springs, Colorado

X-734-67-368

OPTIMAL CONTROL APPLICATIONS FOR ELECTROTHERMAL MULTIJET SYSTEMS ON SYNCHRONOUS EARTH SPACECRAFT

William C. Isley

August 1967

Goddard Space Flight Center
Greenbelt, Maryland

Submitted to AIAA Electric Propulsion and Plasmadynamics Conference
September 11-13 Colorado Springs, Colorado

OPTIMAL CONTROL APPLICATIONS FOR ELECTROTHERMAL MULTIJET SYSTEMS ON SYNCHRONOUS EARTH SPACECRAFT

William C. Isley
Head, Systems Analysis and Ion Propulsion Section
Goddard Space Flight Center
Greenbelt, Maryland

Abstract

The application of multijet electrothermal systems for three-axis attitude control and station keeping of 24 hour synchronous communication satellites is studied in a versatile system simulation that uses operational propulsion system hardware in closed loop tests.

Mission parameters require precise slewing capability to meet antenna fine pointing to $\pm 0.1^{o}$ in limit cycle mode over the full earth disc. Using coupled three-degree-of-freedom attitude equations and disturbance torques, an optimal control policy is synthesized for the slewing maneuver having a performance index based upon time optimal, propellant/power optimal, and weighting of attitude rates.

For constant mass flow propellant feed systems, thrust level degradation was shown to drastically influence both maneuvering time and propellant consumption. A typical case involved a nominal 3 minute slewing time for a pointing vector excursion of 6 degrees. With constant mass flow feed, actual thruster tests produced 40% degradation in thrust level over a period of approximately 8 minutes required to complete the maneuver. By alteration of performance index, near-optimal behavior was approached yielding a slewing time of 4.2 minutes, which is equivalent to the average control impulse. Control stability was demonstrated for thrust degradation in excess of 75% of nominal values.

Preface

The author would like to express appreciation for the support provided by certain individuals in performing the study program described herein. Programming and operation of hybrid computer equipment was capably handled by Computing and Software, Incorporated, under direction of Mr. Drew Dinsmore. Assistance in formulation of the Optimal Control Policy and programming of the digital computer was provided by Mathematical Sciences Group of College Park, Maryland, under NASA Contract NAS 5-10349. Special thanks is due to Dr. Stephen Jones, Thomas Englar, and E. V. Schumann of MSG for their valuable advice in mathematical model development and system checkout.

Introduction

The use of 24 hour equatorial synchronous spacecraft for communications and earth observation has already been demonstrated by Syncom and the Applications Technology Satellite programs. More advanced applications are now under study where large dish antennas would be employed for high gain communication between satellite and ground links. To optimize power requirements for such missions at the high frequencies involved, it is necessary to maintain narrow beamwidths of the order of 0.1 degrees or less. At synchronous altitude the entire earth disc is contained within a cone having solid angle of approximately 17 degrees. A spacecraft positioned at a given synchronous longitude would be capable of communicating with selected regions on the earth surface during the fine pointing mode and, by slewing commands, could re-direct the high gain antenna to new sub-satellite regions. One natural choice for attitude sensing would be a north reference to Polaris and local vertical from IR earth disc trackers. This approach was followed in the subject study program. An alternative and promising approach would be to utilize communication antennas directly in establishing attitude error signals. There are many potential applications for such a spacecraft. The high gain, narrow beam feature of the oriented antenna has direct impact upon deep space missions where power optimization becomes critical. Other possibilities include earth resources mapping, direct broadcast, navigation, and meteorology. Such a spacecraft offers many opportunities for technological development in control systems and communications in addition to the direct applications. Propagation of high frequency signals through the atmosphere, potential use with laser communications, and performance of large dish reflectors are but a few items mentioned here. One basic objective in assessing optimal control for such missions has been to demonstrate that one can obtain desired control stability, while at the same time providing parameter optimization and open-loop adaptive capability. Stability implies maintaining active control over wide variations in plant constants and external disturbances. Optimization implies allowing the option to specify slewing time, propellant to be expended, or maximum rates to be permitted. Open-loop adaptive control implies the ability to alter dynamic performance by ground command in order to maintain near-optimization following severe plant changes or variations in external disturbances. The control system implementation described herein possesses all of these features and also promises to require relatively small on-board spacecraft computers for missions studied.

Attitude control for such a mission can be included under three basic catagories: (1) Acquisition Control, (2) Slewing Mode Control, and (3) Fine Pointing Mode Control. The first category applies from the point of injection of the spacecraft into a near-synchronous orbit through deployment and removal of final injection errors to the point of sensor acquisition. The second category refers to attitude control exercised between two stages of fine pointing mode control, which is under category three. This paper examines only performance aspects during the slewing control mode.

Spacecraft and Propulsion System Description

The spacecraft design concept is based upon spin stabilization during ascent and injection phases during which time a folded configuration is maintained for antenna and solar paddles. Following despin, deployment, and sensor acquisition, the spacecraft configuration in side view would appear as shown in Figure 1. The 30 foot parabolic reflector is directed along the Z-axis, which is an earth-pointed reference. The two solar paddles are supported along the north-south spacecraft axis and oriented in two orthogonal planes in order to minimize variations in power output throughout each orbit. Paddle size was selected to provide a reference power of 300 watts minimum for experiments and auxiliary sub-systems. The large equipment compartment contains a Resistojet Propulsion System which provides required control torques for fine pointing, slewing and station keeping functions (east-west and north-south). The small equipment compartment houses the coarse and fine attitude sensors, tracking-telemetry and command antennas together with associated electronic components. Attitude information is extracted from the Polaris and earth trackers, where angular rate information is obtained indirectly from position signals. Sun sensors are employed during initial acquisition and serve as a backup during normal operation.

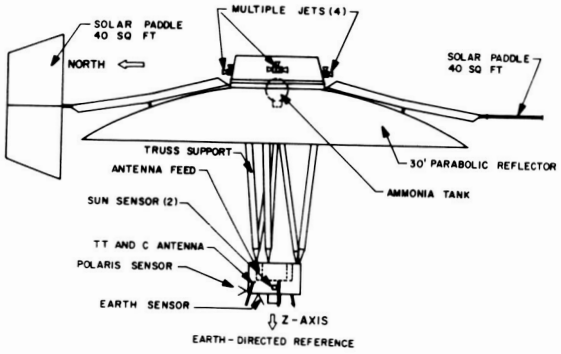

SPACECRAFT CONFIGURATION-SIDE VIEW
FIGURE 1

Four thruster modules are located on the large equipment compartment, each module containing a single resistive heater element and four jet flow passages. Figure 2 presents a top view of the spacecraft indicating schematically the jet locations. A single propellant tank is assumed with manifolding to each of the four multijet modules. Spacecraft structural layout studies for this configuration have shown that the composite center of mass will fall somewhere between the two equipment compartments, resulting in the problem of imparting translational force without introducing attitude disturbance torques. Three alternatives were explored. The first approach is to locate thruster modules as attachments to the rib structure of the antenna at points where jet firings would be along principal axes and through the center of mass. The second approach is to cant each module while mounted on the equipment compartment to a point where pure translational force is achieved. The third approach is to mount all modules symmetrically on the large equipment compartment and balance attitude disturbances with opposing jets. The first approach requires flexible connections in the feedlines with special mounting provisions for each module. Although optimum from the propulsion and control requirement standpoint, it was concluded that too many design problems would be encountered in this approach. The second alternative of canting each module would improve propellant comsumption over that obtainable using approach 3 by as much as 25% during station keeping operation, but would remove jet redundancy for attitude control. If only east-west station keeping were required, a clear choice would be approach 3 as the predominant delta V requirement lies in north-south correction. If, however, north-south is an ultimate requirement for station keeping, the final selection would be a tradeoff in jet locations, weight, and redundancy. It would be possible to add single jets for the north-south requirement without substantially influencing weight. The choice for this study program was approach 3. The thruster type selected was a thermal storage resistojet. An engineering prototype version of the multijet thruster is shown in Figure 3. The concept features a single heater element for use with four jet flow passages. A detailed description of this thruster may be found in Reference 1.

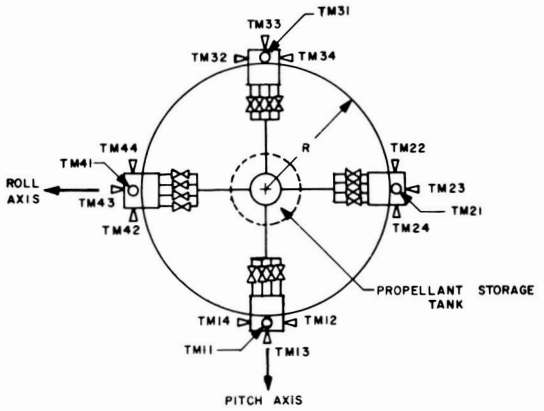

SPACECRAFT RESISTOJET LOCATIONS-TOP VIEW
FIGURE 2

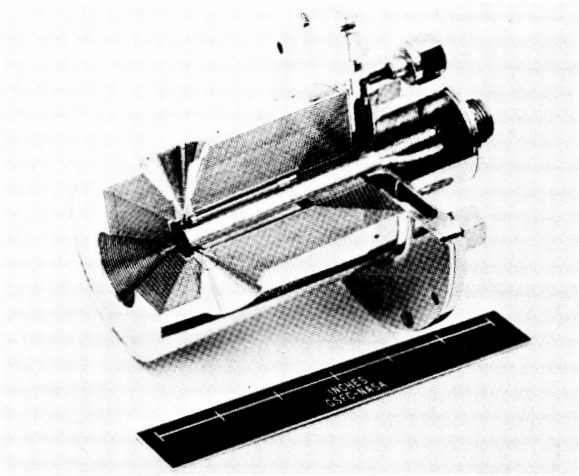

MULTIJET THRUSTER PROTOTYPE
FIGURE 3

Ammonia was selected as the propellant for the resistojet system. Two feed system concepts were studied and tested experimentally during this program. Both approaches are shown in Figure 4. Approach A uses a sonic metering orifice to maintain constant propellant mass flow rate. This type is characterized by a dropoff in thrust during extended jet on-times when conditions are such that heat input is insufficient to maintain exit propellant temperature. For short term pulse mode operation, thermal energy stored can be adequate to maintain relatively constant propellant specific impulse. Approach B employs a pressure regulated feed system. In this case thrust level would remain essentially constant over extended jet on-time and propellant mass flow would increase to compensate for reduction in the realizable specific impulse. The first approach has higher inherent reliability, but lacks flexibility and introduces problems in control due to allowing for thrust level variations. Approach B has greater design difficulty and presents potential reliability problems, but has flexibility in establishing levels of pressure regulation compatible with different sizes of control jets and in maintaining constant thrust output. An objective of this study was an assessment of each of these concepts from the controls standpoint to establish any effect upon stability, and parameter optimization under optimal control policies.

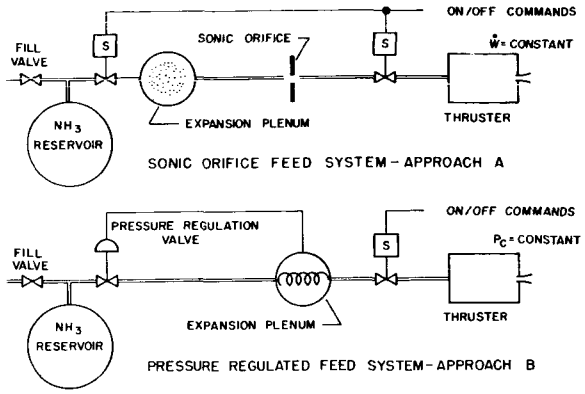

ALTERNATE FEED SYSTEM CONCEPTS
FIGURE 4

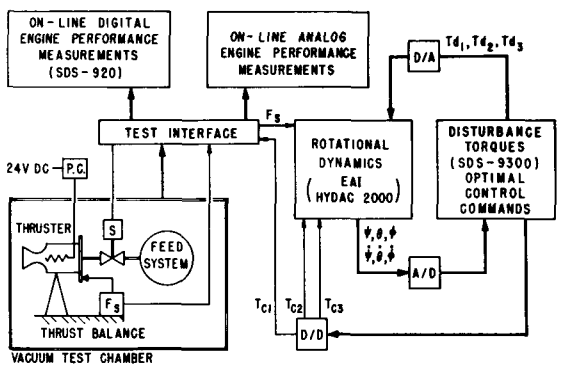

SIMULATION / TEST FLOW DIAGRAM
FIGURE 5

The large number of variables confronted in this study made it necessary to establish a reference design for the spacecraft and propulsion system. The physical constants used in this design are presented in Table 1.

Simulation/Test Equipment and Approach

The optimal control studies were performed using digital-analog hybrid computer equipment tied in a closed-loop manner with propulsion system hardware under test in a thermal vacuum chamber. Figure 5 presents a flow diagram for the overall simulation and test complex. An EAI Hydac 2000 computer was employed for generation of spacecraft rotational motions in three axes. The six Euler state variables were subjected to analog-to-digital conversion and then were used as inputs to an SDS-9300 digital computer which executed optimal control commands. This computer was also used for generation of disturbance torques which were processed through digital-to-analog conversion and then routed to the Hydac 2000. The accuracy of both A/D and D/A channels was 15 bits (binary). A digital-to-digital interface was utilized for execution of the thruster on-off commands in each axis. The roll axis signal (T_{c1}) was used in the full simulation stage to operate actual thruster hardware during test conditions. This was accomplished through use of a test interface which permitted both analog and digital communication between the computer laboratory and the vacuum laboratory. Thrust was measured directly in these tests by means of a high frequency balance whose output signal was processed and routed as a feedback to the Hydac 2000 computer. Both on-line digital and on-line analog engine performance measurements were taken. The digital system consisted of an SDS-920 computer which multiplexed

TABLE 1

SPACECRAFT REFERENCE DESIGN CONSTANTS

AXIS	DESIGNATION	RATED THRUST(lbs.)	MOMENT ARM(ft.)	TORQUE(ft.-lbs.)	MOMENT OF INERTIA(slugs-ft^2)
pitch	θ	0.026	4.6	0.12	2000
roll	ϕ	0.017	4.6	0.08	3580
yaw	Ψ	0.011	3.6	0.04	1970

NOTE: Above thrust and torque values for the yaw axis assume a couple.
Moment of inertia values are for the principal axes.
Maximum thruster misalignment angles are 1 degree in each axis.

analog voltages from the engine experiment and then converted these signals to digital form and ultimately to binary tape. This information was utilized during post operation phases for extensive data analysis on the hardware. Three temperature measurements were taken from the thruster body to establish heat shield efficiency. Thruster chamber pressure was measured separately and converted to digital form at 10 millisecond intervals during each run. Thruster core temperature readings were obtained in a similar manner. Propellant mass flow rate was obtained by use of a calibrated volume storage sphere, where pressure and temperature versus time histories were used to compute fuel expended. During preliminary tests this technique was compared with readings of a wet test meter for nitrogen propellant, and it was found that mass flow rate could be predicted readily to within 3%. In actual simulation tests tank pressure and temperature signals were routed to the EAI 231R analog computer where mass flow rate and specific impulse were computed directly in real time. Results of such tests were also checked against thrust as calculated from the thruster chamber pressure output. Agreement was excellent. A Hall-effect constant power dc-dc conditioner was constructed to regulate the resistojet heater during test runs. As the heater element tends to cool over an extended pulse, it is necessary for this regulator to vary current to compensate for power fluctuations. A number of performance measurements were also recorded by analog means to serve as further check on the digital results. Output information was displayed by strip chart records in analog form, as well as by digital plotter and printer from the SDS-920 computer. The test interconnections required approximately 100 feet of cable between computers and the vacuum test installation. Noise levels and early ground loops necessitated both shielding and isolation of leads. LC filters were employed to obtain signal-to-noise ratios in excess of 90 to 1. This paper does not permit a discussion of engine performance results other than those directly associated with the optimal control problem. Applicable performance data is described in a later section dealing with Simulation/Test Results.

The general approach followed three basic phases of investigation. The first phase dealt with a full three axis hybrid simulation of optimal and sub-optimal slewing maneuvers using "ideal" thruster and sensor components. The second phase introduced simulated "real effects" for the resistojet, including transport delay, rise/tailoff behavior, and feed system characteristics. The third phase substituted actual prototype hardware into one axis of the three axis simulation. Figure 6 presents a photograph of the prototype thruster under test in the thermal vacuum chamber during the third phase of this program. The view shown includes the thrust balance in place and operation from an external feed system.

Spacecraft Dynamics Model

The mathematical model for spacecraft rotational dynamics employed in this study is based upon an assumption that the composite structure (including antenna and solar paddles) can be represented as a single rigid body. Angular motions are described by nonlinear Euler equations for principle axes of inertia with transformation into an

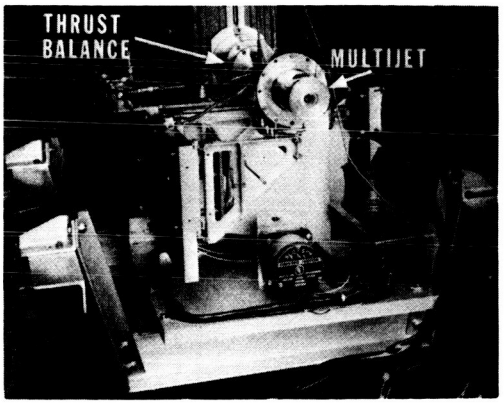

FIG. #6 THRUSTER TEST ARRANGEMENT

Euler sequence of rotations. The general system of equations is shown in Figure 7. The terms ($\omega_1, \omega_2, \omega_3$) represent inertial body rates about roll, yaw, and pitch axes, respectively. The dot superscripts denote time derivatives. Terms (I_1, I_2, I_3) are principal moments of inertia. Control torques are expressed as (T_{c1}, T_{c2}, T_{c3}) about each of the axes. The disturbance torques include effects of solar radiation pressure, gravity gradient, and thruster misalignments with respect to principal axes. These composite terms are represented by (T_{d1}, T_{d2}, T_{d3}). The next three equations provide the selected Euler angle sequence. Initial studies were performed with the full nonlinear dynamics. A substantial number of analog components were found to be necessary to provide the complete simulation, primarily due to the number of matrix transformations involved in generating the various reference angles. Certain simplifications were attempted and found to be very good approximations. Small angle approximations were tried for the Euler transformation, and it was found for cases studied that influence upon spacecraft motions was negligible. To free computer equipment for other required computations, a reduced system of nonlinear equations was used for the remaining study program. These equations are presented in (7) through (9).

$$I_1\dot{\omega}_1 = (I_2 - I_3)\omega_2\,\omega_3 + T_{CI} + T_{DI} \quad \text{----------(1)}$$

$$I_2\dot{\omega}_2 = (I_3 - I_1)\omega_1\,\omega_3 + T_{C2} + T_{D2} \quad \text{----------(2)}$$

$$I_3\dot{\omega}_3 = (I_1 - I_2)\omega_1\,\omega_2 + T_{C3} + T_{D3} \quad \text{----------(3)}$$

$$\dot{\phi} = \omega_1 - \text{TAN}\,\psi\ \text{SIN}\,\phi\,\omega_2 - \text{TAN}\,\psi\ \text{COS}\,\phi\,\omega_3 \quad \text{----(4)}$$

$$\dot{\psi} = -\text{COS}\,\phi\,\omega_2 + \text{SIN}\,\phi\,\omega_3 \quad \text{----------(5)}$$

$$\dot{\theta} = \text{SEC}\,\psi\ \text{SIN}\,\phi\,\omega_2 + \text{SEC}\,\psi\ \text{COS}\,\phi\,\omega_3 \quad \text{-------(6)}$$

$$\dot{\phi} = -\omega_3\,\psi + \omega_1 \quad \text{----------(7)}$$

$$\dot{\psi} = \phi\,\omega_3 - \omega_2 \quad \text{----------(8)}$$

$$\dot{\theta} = \phi\,\omega_2 + \omega_3 \quad \text{----------(9)}$$

GENERAL SPACECRAFT DYNAMICS MODEL
FIGURE 7

Coordinate Systems

A total of seven orthonormal coordinate systems were employed to describe the spacecraft dynamics in terms of target conditions.

Inertial Earth-Fixed Reference

The E system represents the inertial reference whose origin is located at the mass center of the earth and whose unit vectors (e_1, e_2, e_3) form a right-handed coordinate frame. Direction e_1 points to the First Point of Aries on the equator; e_3 points through the north pole; e_2 is chosen perpendicular to the e_1 e_3 plane to complete the orthogonal system. The E system does not rotate with the earth.

Moving Earth Reference System

The M System denotes a right-handed orthogonal frame wherein the origin lies at the earth mass center. The unit vectors (m_1, m_2, m_3) are taken such that m_3 points through the north pole; m_1 and m_2 always lie in the earth equatorial plane. Unit vector m_1 will rotate with respect to e_1 at the earth rotational velocity.

Spacecraft Position Reference

The S system is employed to define the spacecraft position in terms of the earth-fixed reference frame. The origin of this system lies at the center of mass of the spacecraft, and the unit vectors (s_1, s_2, s_3) form a right-handed coordinate frame. Unit vector s_2 is directed along the local vertical to the earth center; s_3 is taken positive in a direction toward the north; s_1 is directed perpendicular to the s_2 s_3 plane being positive in the direction of the velocity vector.

If the spacecraft orbit lies in the equatorial plane and is circular, then s_3 is directed through the earth north pole. If the orbit altitude is selected to be the 24 hour synchronous condition, one can state that the angular velocity of the S system relative to the E system is simply equal to the earth rotational rate. In the following discussion, angular motion about s_3 is considered to be pitch motion; that about s_1 will be roll motion; and that about s_2 will be yaw motion.

Attitude Reference System

The R system defines the target attitude conditions for the spacecraft. Its origin coincides with that of the S system and the unit vectors (r_1, r_2, r_3) form a right-handed coordinate frame. Unit vector r_2 points positive to the earth target; r_3 is taken perpendicular to r_2, and the angle between s_3 and r_3 is taken to be the minimum value; unit vector r_1 is taken perpendicular to the r_2 r_3 plane so that the R system has orthogonal bases. The angles between the R system and the S system establish target values for antenna pointing in terms of the earth-fixed reference frame. Figure 8 presents a geometrical picture of the E, M, S, and R coordinate systems.

Spacecraft Body Fixed Reference System

The B system defines a reference frame rigidly attached to the spacecraft structure, used for the purpose of introducing thruster misalignments with respect to the principal axes. The origin of the B system lies coincident with that of the S system and the unit vectors (b_1, b_2, b_3) are selected arbitrarily to match thruster locations and to form a right-handed orthogonal reference.

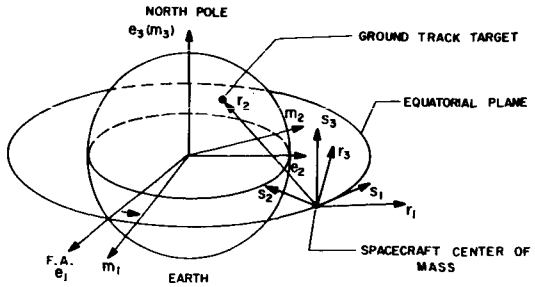

REFERENCE COORDINATE SYSTEMS
FIGURE 8

Spacecraft Principal Inertia Reference System

The P system denotes a right-handed frame so positioned that the unit vectors lie along the three principal axes of inertia of the spacecraft. To preserve continuity of indexing, the subscripts (1, 2, 3) are taken along body principal axes 1, 2, 3 shown in Figure 7.

Ground Track Reference System

The G system denotes a right-handed frame so positioned that longitude and latitude points of intersection of b_2, with the surface of the earth can be defined. The G system origin lies at the center of the earth. Unit vectors (g_1, g_2, g_3) form an orthogonal set. Unit vector g_1 is directed in a positive sense through the point of intersection with b_2; g_3 is taken positive to the north; g_2 is perpendicular to the g_1 g_3 plane parallel to the direction of the velocity vector.

Disturbance Torques

Solar radiation torque was assumed to act only upon the two flat solar paddles and the 30 foot dish antenna. A rigorous digital program was prepared for the SDS-9300 computer to allow prediction of torque levels on each body axis as a function of orientation, shadowing, and absorptivity/emissivity properties of the structure.

For simplicity in simulation during individual slewing maneuvers, the sun line angle relative to the E system was taken to be constant. This assumption was assessed during early experimental runs and found to be well within overall accuracy requirements for this study. For a six minute slewing period, sun line movement would be approximately 0.004 degrees.

Gravity gradient torques were programmed for the SDS-9300 computer using equations developed by C. C. Barrett of Goddard Space Flight Center in NASA Technical Note TND-3652.

Mathematical model development for each of the above torques is fully covered in Reference 2, together with digital program listings for the SDS-9300 computer.

The mathematical model included provision for introduction of thruster misalignment angles taken

with respect to the principal axes. A maximum value of 1 degree was selected as a reasonable limit for such disturbances.

Control Torques

Jet firing commands consist of on-off signals received from the optimal control computer. The control action may then be described as a bang-off-bang system. For purposes of simulation of an "ideal" thruster, it was assumed that the thrust pulse was a square wave. Characteristic profiles for simulated "real" thrusters were obtained by operating the actual hardware under vacuum and then reproducing rise profile, delay constants, tailoff during thrust, and final tailoff following thrust-off command.

Optimal Control Synthesis

The optimal control problem may be stated in the following manner: a slewing maneuver involves total re-alignment of the pointing vector to the required target location and at rest with respect to the S system. The slewing maneuver is to be performed such that a prescribed performance index is satisfied in terms of minimizing slewing time, propellant required, maximum rate experienced, or some combination thereof. For a specified time of arrival (which can be set at a minimum value) the objective is to minimize total propellant consumed while adhering to a maximum angular rate limitation. Such a control formulation can be synthesized using the equations presented in Figure 9.

$$\dot{\boldsymbol{\omega}} = \mathbf{I}^{-1}\mathbf{u} + \mathbf{b} \qquad \text{(10)}$$

$$A(\xi)\dot{\xi} = \boldsymbol{\omega} \qquad \text{(11)}$$

$$\mathbf{y} = \mathbf{I}\,\boldsymbol{\omega} \qquad \text{(12)}$$

$$A(\xi) = \begin{bmatrix} 1 & 0 & \sin\psi & \\ 0 & -\cos\phi & \sin\phi & \cos\psi \\ 0 & \sin\phi & \cos\psi & \cos\phi \end{bmatrix} \qquad \text{(13)}$$

$$J = \begin{bmatrix} \int_{t_0}^{t_1} (\lambda_{11} + \lambda_{12}\,|u_1| + \lambda_{13} y_1^2)\,dt \\ \int_{t_0}^{t_1} (\lambda_{21} + \lambda_{22}\,|u_2| + \lambda_{23} y_2^2)\,dt \\ \int_{t_0}^{t_1} (\lambda_{31} + \lambda_{32}\,|u_3| + \lambda_{33} y_3^2)\,dt \end{bmatrix} \qquad \text{(14)}$$

CONTROL SYNTHESIS EQUATIONS
FIGURE 9

Equations (10) and (11) express in a convenient vector form the spacecraft dynamics where $\boldsymbol{\omega}$ has components $\omega_1, \omega_2, \omega_3$ along the body principal axes of inertia; $\mathbf{I}$ represents the inertia dyadic; $\mathbf{u}$ is the control vector having components u_1, u_2, u_3 along body fixed axes; ξ represents a vector whose components are the Euler angles (pitch, yaw, roll); the vector $\mathbf{b}$ includes perturbations from disturbance torques and second order terms in inertial cross-coupling. The $\mathbf{b}$ vector has components b_1, b_2, b_3 along the body axes. Equation (12) is an expression of the angular momentum vector. Equation (13) is the Euler angle transformation, whereas $\dot{\xi}$ denotes the Euler rates having components along each of the body axes. Equation (14) denotes the J vector which is used to obtain a performance index of optimal control behavior. The minimization of integral components of J forms the basis of control system optimization. The term, t_0, represents initial time and t_1 final time for a given maneuver. The terms λ_{ij} represent weighting parameters for system performance variables, where λ_{i1} weights time optimality with respect to axis (i). Parameter λ_{i2} weights fuel optimality with respect to axis (i), and λ_{i3} constrains maximum angular rate about axis (i).

The unique feature of this optimization scheme is that a non-linear six degree of freedom system is split into three separate systems, each having two degrees of freedom. This is achieved by a non-linear change in variables. The resulting (lower order) systems are amenable to closed-form synthesis through the use of Pontryagin's Maximal Principle. The optimal synthesis for the total system equations is achieved by a process of "time synchronization" of the lower order systems wherein the weighting parameters are adjusted through sampled-data feedback of the state variables to permit each axis to arrive on target simultaneously. The detailed mathematical development is presented in Reference 2 and is too involved for further discussion herein.

For purposes of illustration, however, one may examine phase plane trajectories of the lower order systems. Figure 10 presents typical time optimal trajectories in three axes for two conditions. Trajectories labeled A (solid lines) represent cases where external torques and/or cross-coupling have a negligible effect upon dynamics. Cases labeled B (dotted lines) indicate what is to be expected when such nonlinearities are not insignificant. Note that axis 1 is driven continuously to the target, whereas axes 2 and 3 to effect a fuel economy enter a coasting phase. This is a result of the time synchronization process. External torques and Euler cross-coupling are accounted for directly in the optimal control strategy and result in modified trajectories as shown in the figure. This feature can be significant in effecting fuel savings in the presence of high external torques and/or high initial angular rates.

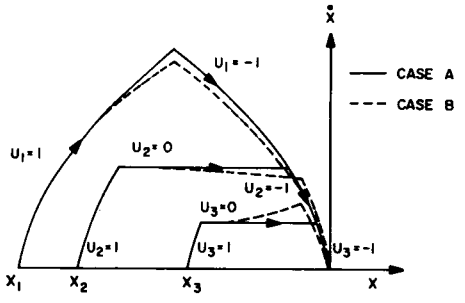

TIME SYNCHRONIZATION PHASE PLANE BEHAVIOR
FIGURE 10

Simulation and Test Results

Phase I - Simulations Involving Ideal Thruster

The first simulation phase assumed use of ideal thrusters and sensors. Using reference design constants from Table 1, parametric cases were studied varying the three weighting factors in the performance index in conjunction with initial and final values of attitude position and rates on each of the three axes. The phase plane diagram was employed to represent the resulting trajectories. Figure 11 presents the case of a 140 degree ground track maneuver chosen to originate at 70 degrees south latitude and 100 degrees west longitude and end at 70 degrees north latitude and 100 degrees west longitude. For these runs the spacecraft is positioned at a longitude (equatorial) of 100 degrees west. This slewing maneuver can be accomplished by a single roll action. The initial roll rate was arbitrarily selected to be zero. The case $\lambda = 1, 0, 0$ represents the time optimal response. The maximum roll rate experienced was slightly in excess of 1.43 degrees per second. The roll axis arrived on target without experiencing overshoot. The second trajectory demonstrates a run where some weighting is applied to propellant expended ($\lambda = 1, 2, 0$) but where maximum rate is not restricted. In this instance the positive roll jet is actuated at time zero and remains on until the position reaches approximately 15.5^{o} from the target whereupon the control turns off the roll jet. It remains off and in a coasting mode until the position reaches approximately 1.6^{o} from the target whereupon the negative roll jet is activated driving the roll rate to zero at the target position. The third trajectory demonstrates the influence of the weighting factor upon maximum angular rate. It was found that the propellant weighting factor could be adjusted to yield trajectories equivalent to those given a maximum rate limit. This reduces weighting factor commands to only time and propellant. The 140 degree maneuvers were repeated to ascertain the effect of reducing actual thrust level under conditions where the control logic was based upon full rated thrust. The results of these runs are shown in Figure 12. Here, a 75% reduction in actual thrust was programmed into the computer. It is interesting to note that the system remained stable under these conditions in spite of experiencing two overshoots prior to arrival on target. The maximum angular rate was slightly lower than the ideal case, and time required to reach target increased accordingly. Runs similar to those shown were performed during this phase, and it was found that the control law was inherently stable throughout the entire operating range until control torque was reduced to the level of disturbance torques. From Figure 12 it is apparent that, without an open-loop adaptive feature of some sort, partial failure of a jet (loss of thrust) could result in propellant consumption penalty due to the overshoot. There is, however, a way to correct for such performance using the subject optimal control policy. By ground command, the control torque constant can be adjusted to return the phase plane behavior back near the ideal case where overshoot can be eliminated. The concept of time synchronization, described in the previous section was shown to substantially reduce any influence due to Euler and inertial cross coupling. In order to present meaningful comparisons, a slewing maneuver from the Mojave tracking station in the United States to the Quito station in Equador was used to establish performance curves. Figure 13 presents the time optimal phase plane trajectories for roll, pitch, and yaw axes for this case, where external torques, and cross coupling terms are included. The use of time synchronization provides a second order (sub-optimization) on propellant consumed since it is not important that any one axis be on target prior to the remaining two axes. The influence of nonlinearities is compensated for by the sampled-data adjustment of the bias constant in the switching functions. The next important tradeoff is one involving fuel expended versus slewing time for parametric values of performance weighting factors. This is shown in Figure 14. The standard torque curve was generated using the reference design constants from Table 1. At $\lambda_{2=0}$, the slew will be accomplished in a time optimal manner. As increasing values of this weighting factor are assigned (using a constant fuel weighting factor) the slewing time increases and fuel required reduces. The exponential nature and range of the abscissa definitely show that significant relative savings are possible by proper choice of weighting constants.

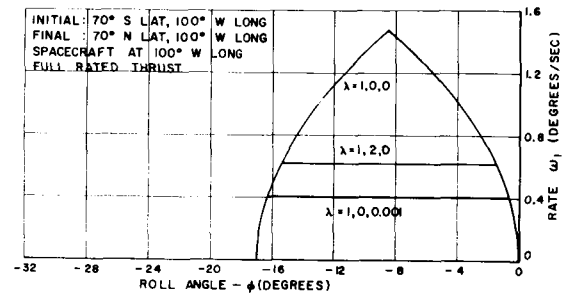

PHASE PLANE 140 DEGREE GROUND TRACK MANEUVER
FIGURE 11

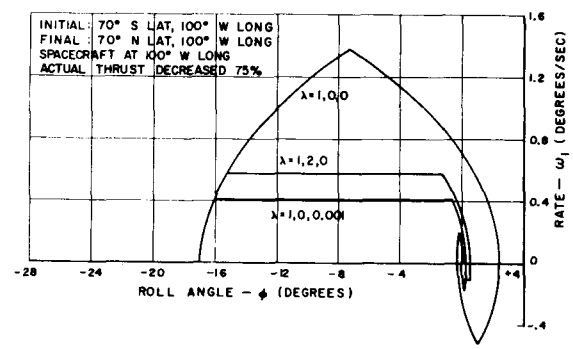

PHASE PLANE 140 DEGREE GROUND TRACK MANEUVER
FIGURE 12

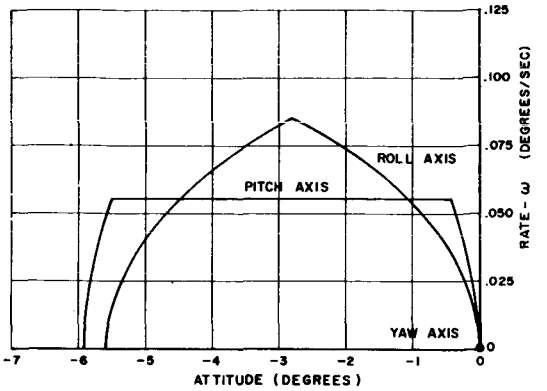

THREE AXIS PHASE PLANE - MOJAVE TO QUITO
FIGURE 13

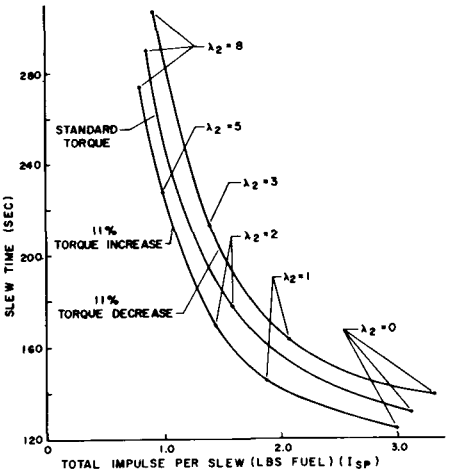

TIME - FUEL CURVES FOR IDEAL THRUSTER
(MOJAVE - QUITO)
FIGURE 14

For example, a cold gas propellant having a specific impulse of 60 seconds would require slightly in excess of 0.05 pounds consumed per slewing maneuver between Mojave and Quito. For a reasonable estimate of 100 maneuvers per mission this would come to 5 pounds of fuel required just for this operation. By permitting the slewing interval to increase from 131 seconds in the subject case to 280 seconds, a three to one reduction is possible in fuel used. For the resistojet, average specific impulse values in the range of 240 seconds have been obtained over operating periods of 130 seconds at power levels of 30 watts or less using the thermal storage concept. This would decrease relative fuel penalty by a factor of about three-fourths. Even in this case, 1.25 pounds of fuel would be required for 100 slewing operations. This figure could well go as high as 5 pounds for large disc maneuvers. Two other curves are shown. One indicates effect of increasing control torque by 11% over reference values and the other by decreasing control torque in the same amount. Note the substantial influence of the control torque parameter near the vicinity of optimal time maneuvers. Torque increase thus effects a fuel economy and should be used as a tradeoff parameter in system design. Figure 15 presents the time traces of pitch and roll axis angles during the Mojave-Quito slew. These traces are of interest in that they show the effect of time synchronization upon achieving near-optimal behavior. The pitch axis jet is turned off for a major portion of the slewing maneuver in order to match arrival times in both axes. The roll attitude deviation shown is due to the large difference in moments of inertia on the two axes.

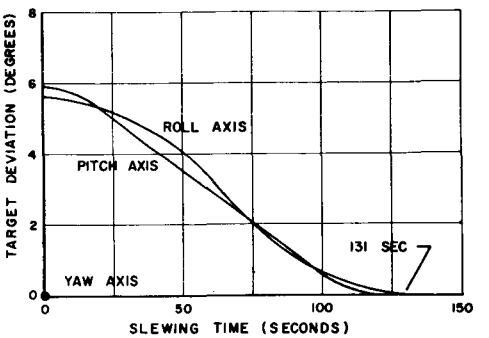

TIME HISTORY - SLEWING ANGLES - MOJAVE TO QUITO
FIGURE 15

Figure 16 presents the longitude-latitude ground track between the two stations. It was of considerable interest that time optimal maneuvers create the greatest deviation from a great circle path between the two points. As propellant is weighted more heavily the deviation becomes less pronounced and approaches a straight line approximation. The same behavior was obtained by weighting of maximum allowable rates on pitch and roll axes. The optimal control model permits another interesting possibility for generation of predetermined ground tracks. This is accomplished by generating the target reference coordinates as an input (time varying) to the optimal computer. By adjustment of the weighting parameters, it is possible to closely follow a pre-selected path at prescribed angular rates, and to arrive on any target at predetermined time.

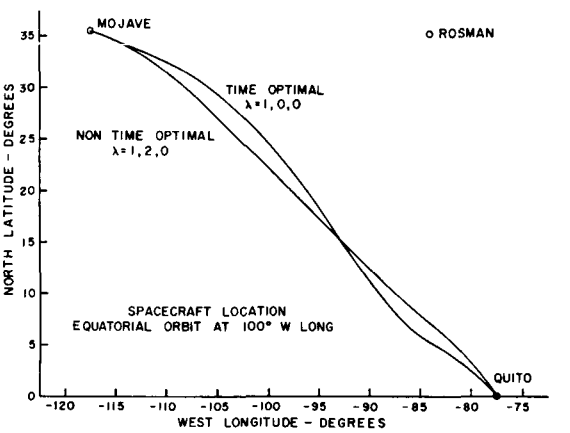

GROUND TRACK MOJAVE TO QUITO
FIGURE 16

Phase II - Simulations Involving Real Thruster Effects

The second phase of simulation involved substitution of real thruster effects into the mathematical model. Using the constant mass flow feed system approach, a series of thruster component tests were conducted to characterize thrust-time behavior over periods ranging up to 10 minutes. For a constant power input of 30 watts it was

found that measured thrust degraded by 40 percent at the end of an 8 minute continuous pulse. A simulation run was performed using bang-bang position error correction for a typical 6 degree roll angle excursion of the pointing vector, where thrust produced by constant mass flow feed was assumed. This was compared with results using optimal control policy taken for an "ideal" thruster exhibiting constant thrust level over this period. The ideal case required a nominal 3 minute slewing time for the weighting parameters employed. Substitution of the "real effects" model and non-optimal control produced four overshoots prior to final target acquisition. The slewing time increased accordingly to approximately 8 minutes. This was followed by substitution of near-optimal control using $\lambda_{2=0}$ as shown in Figure 17. Slewing time was reduced to 4.2 minutes for the time optimal weighting. Other performance weightings are also shown, and it is evident that a value near $\lambda_2 = 0.5$ is the best time optimal case for the subject real thruster effects. As weighting is further increased, slewing time substantially increases as fuel consumed is decreased. These cases were generated using maximum rated thrust (F_R) of the jet as the constant (F_C) in the optimal control model. Figure 18 indicates the effect of reprogramming F_C so that it is equal to 0.7 F_R in the control model. Now, time optimal weighting (i.e. $\lambda_2=0$) occurs very close to the time optimal condition. This method of correcting for actual thruster behavior is a powerful one, and can easily be incorporated into on-board spacecraft computers.

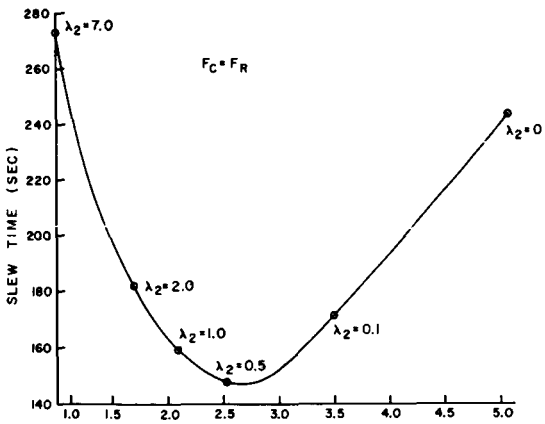

REAL THRUSTER EFFECTS
TIME-FUEL CURVE
(MOJAVE-QUITO)
FIGURE 17

Phase III - Simulations Involving Closed-Loop Actual Hardware Tests

A series of tests were performed where actual thruster hardware was substituted into the roll control loop and measured thrust employed as a direct feedback into the computer simulation. The general block diagram shown in Figure 5 represents inter-relationship of major system elements. For these tests the maximum rated thrust was 0.02 lbs, and the roll axis moment of inertia changed to 3200 slugs-ft^2. A pressure regulated feed system was employed in conjunction with the calibrated volume sphere for determination of mass flow rate. Equations of state for gaseous ammonia as expressed in differential form were integrated in real time

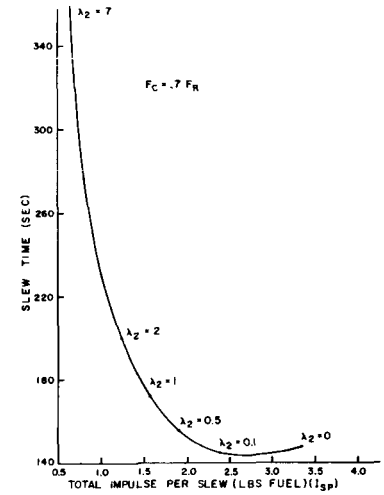

REAL THRUSTER EFFECTS WITH MODIFIED CONTROL
TIME-FUEL CURVE (MOJAVE-QUITO)
FIGURE 18

on the EAI 231R computer to obtain mass flow and then combined with the thrust measurement to establish specific impulse. The SDS-920 computer recorded all measured engine variables for post operation data processing. Both hot flow and cold flow data was obtained.

In the cold flow tests, signal to noise ratios for thrust and pressure-temperature measurements were better than 90 to one. It was found in the hot thruster tests that the thrust balance noise level was substantially affected by thruster operating temperature and temperature variations. By filtering, it was possible to obtain a thrust S/N ratio of 10 to 1. As of this writing, hot thruster tests are incomplete and further noise reduction is necessary for the thrust balance. To illustrate the overall simulation system capability, results of cold flow thruster tests are presented herein. Figure 19 is a plot of the roll axis phase plane which was generated during a closed-loop, three axis test. Note that one overshoot resulted in the trajectory prior to reaching target destination. This was attributed to some variation actually experienced in thrust output over the run. Further tests pointed to lack of adequate pressure regulation as the source of this problem. The single overshoot can be readily removed by adjustment of the control constants in any event. Figure 20 presents time histories of propellant flow rate, thrust, and specific impulse during the cold flow thruster test. The dotted line shown in the thrust-time trace is meant to represent the actual condition where the opposing roll jet is activated during the slewing maneuver. Calculated specific impulse remained essentially constant throughout the run at 100 seconds. There appeared to be considerable rise and tailoff associated with the selected thruster-feed system configuration. No attempt was made in this program to reduce these time constants, but for short term pulse mode application (as in the fine pointing mode) such improvements would be necessary to optimize performance.

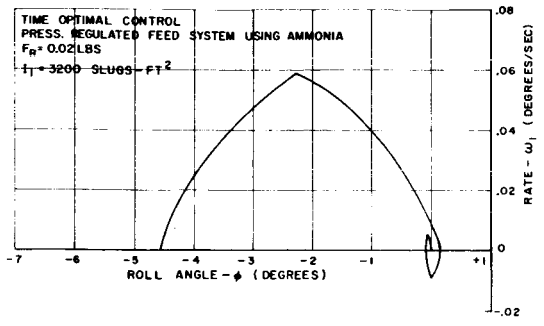

PHASE PLANE-ACTUAL THUSTER PERFORMANCE
FIGURE 19

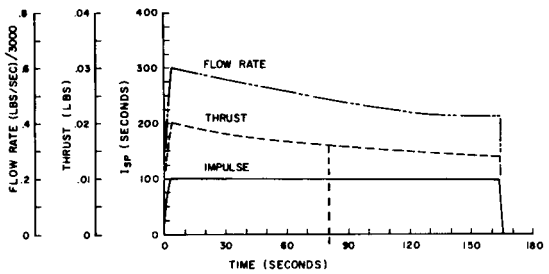

COLD FLOW THRUSTER PERFORMANCE
FIGURE 20

Summary

The value of open-loop adjustment of dynamic performance using the optimal control policy described herein has been demonstrated. For real thruster effects, one can adapt slewing behavior to prescribed conditions by reprogramming of weighting parameters and control constants. To date, only limited assessment has been possible of potential capabilities of this optimal control approach. Preliminary estimates have been made of the required computer size for on-board spacecraft application. The present digital-analog hybrid program required 12,250 octal locations on the SDS-9300 computer. This includes the main program, all required sub-routines for input-output and for disturbance torque computations. This does not include a digital sub-routine for real sensor effects. Programming was performed in Fortran IV using a main executive routine and modular construction. It would require approximately 4370 octal locations for spacecraft application, where unnecessary routines for input-output and disturbance torques are eliminated from requirements. It is further estimated that 3500 octal locations could satisfy the program requirements if machine language programming were employed, and that even further reductions are possible by going to a special purpose (wired-in) computer concept. This core size is considered entirely realistic for spacecraft use in terms of required volume, weight, and power input. Follow-on effort is being directed toward a full implementation of real sensor effects into the dynamics model and extension of the structure concept to include elastic body effects due to antenna and solar paddles. Future applications will include (1) extension of the control model to include a self-adaptive computer in closed-loop for system optimization, and (2) development of optimal tracking or mapping policies where target conditions are expressed as prescribed time functions.

References

1. AIAA Paper 76-622, "Design and Performance of a Thermal Storage Resistojet", R. N. Gibson & T. A. Cygnarowicz, Goddard Space Flight Center

2. Final Report on Synthesis of Optimal Control for Satellite Attitude Maneuvers Prepared by Mathematical Sciences Group, College Park, Maryland, under Contract to GSFC NAS 5-10349.